Mechanical Analysis of Full-Scale Nb3Sn CICC Designs for Tokamaks

Mechanical analysis of full-scale Nb_3Sn CICC designs for tokamaks

R. Riccioli, A. Torre, D. Durville, M. Breschi, and F. Lebon

***Abstract*—Several designs of Nb_3Sn Cable-In-Conduit Conductors (CICCs) have been proposed so far for high-performance tokamak magnets. The Nb_3Sn strands composing the conductors are subjected to mechanical stresses of electromagnetic (EM) and thermal origin, inducing local deformations and affecting the strands critical current carrying capability. In the last ten years a numerical tool based on a finite element (FE) code has been developed to simulate the mechanical behavior of the CICCs subjected to operating loads. The main goal of this tool is to predict the electro-mechanical performance of the conductor in operation as a function of the design parameters such as the void fraction, the twist pitches and the conductor shape.**

In this work, a detailed model of a full-cable ITER TF CICC is presented. This model proves useful for a deeper understanding of the mechanical phenomena occurring among the sub-cables during the conductor operation. Moreover, the numerical modelling of different conductors from the ITER, DTT and JT60 projects is also presented to highlight the versatility of the code.

***Index Terms*— Superconductors, Nb_3Sn, Strain-sensitiveness, Fusion Magnets, Cable-In-Conduit Conductors.**

I. Introduction

In several magnet systems for recent Tokamaks [1], such as ITER currently under assembling in France, the magnet cables are composed of hundreds of composite superconducting wires containing Nb_3Sn, a strongly strain sensitive material [2]. During machine operation, these cables are submitted to cyclic mechanical loads of electromagnetic and thermal nature. It has been observed that these repetitive loads trigger a gradual but steady decrease of the electrical performance of the cable [3], [4]. Up to now, the exact mechanisms relating this macroscopic loss of electrical performance to the local strain state of the superconducting wires are still partially unknown. This issue is extremely complex because of its multi-scale and multi-physics nature. This paper is based on previous works [5]-[7] with the final goal to shed some light on both cable and strand scales by developing a solid numerical electromechanical model to simulate the superconducting cables in operation. The model is meant to identify and understand the causes of performance degradation as well as to obtain a predictive tool to assess cable behavior for new superconducting cables. This work presents the recent upgrade to the numerical model and the main results of the simulations compared to experimental studies.

II. The numerical approach

The numerical approach chosen for this study relies on the FE mechanical code MULTIFIL [8]. The code was adapted for the simulation of fusion cables following the Cable-In-Conduit Conductor (CICC) design. This section presents the major upgrade of the model and the specific numerical protocol that was followed for the MULTIFIL simulations of cables for fusion magnets.

A. Full cable model upgrade

MULTIFIL simulates a set of beams discretized by a 1-D mesh representing the assembly of wires belonging to a cabling stage, or sub-cable, of a cable. This assembly has to be shaped into the desired final geometry, defined by the cable design. MULTIFIL disposes of a set of particular analytical rigid surfaces (either cylinders or planes) interacting with the wires through frictional-contact forces. By moving these rigid surfaces, the cable can be compacted from a theoretical shape of multi-twisted helical trajectories to the final compacted cable or sub-cable. The former model presented in [9] allowed the simulation of one of the six sub-cables, also called “petal”, referring for example to the ITER CS CICC [9]. Moreover, the petal was untwisted, which is quite a critical difference with the real cable. The previous works [6] and [7] focused on the improvements of the single petal model, which is able to provide qualitative information on the mechanical behavior of the conductor in a short computational time. However, the scaling-up is fundamental for the reliability of the model and understanding of the macroscopic phenomena occurring at the cable scale.

The upgrade of MULTIFIL to the full cable model was handled in two steps. The first step led to the development of the twisted petal model: new helical analytical surfaces were coded in the core of MULTIFIL as those shown in Fig. 1a) for an ITER TF sub-cable (see reference data in Table I). It was also necessary to introduce an additional stage in the conductor design, representing the twisting of the petals in the cable hierarchical

Manuscript received November 30th, 2021.

R. Riccioli is with the CEA, Commissariat à l'énergie atomique et aux énergies alternatives, Cadarache, France and also with Aix-Marseille University, France and with Bologna University, Italy (e-mail: rebecca.riccioli@cea.fr).

A. Torre is with the CEA, Commissariat à l'énergie atomique et aux énergies alternatives, Cadarache, France.

D. Durville is with MSSMat Laboratory (Mechanics of Soils, Structures and Materials), Centrale Supélec, CNRS UMR8579, Université Paris Saclay, France.

M. Breschi is with the Department of Electrical, Electronic and Information Engineering, University of Bologna, Italy, Viale del Risorgimento 2, 40136 Bologna, Italy.

F. Lebon is with Aix-Marseille Université, CNRS, Centrale Marseille, LMA (Laboratoire de Mécanique et Acoustique), France).

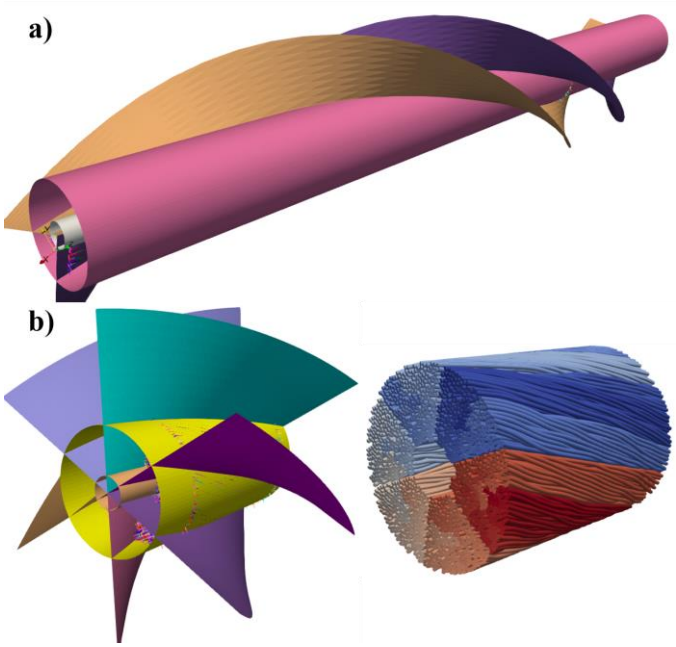

Fig. 1. a) Illustration of helicoid rigid surfaces of a single sub-cable, b) Illustration of helicoid rigid surfaces of the full cable model on the left and of the cable on the right.

TABLE I
ITER TF CIC CONDUCTOR PARAMETERS

Cabling layout	((2sc+1Cu)x3x5x5 +(3x4Cu))x6
Central spiral	8x10 mm
Petal wrap	0.10 mm thick, 50 % cover
Cable wrap	0.10 mm thick, 40 % overlap
Cr coated strand diameter	0.82 mm
Strands number	1422
Void Fraction (annulus)	29.7 %
Mean twist angle	0.297
Cable diameter	39.7 mm
SS 316LN jacket outer diameter	43.7 mm

description. This level is characterized by a helix defined by its radius, initial angle and twist pitch. Hence, this feature is usually necessary when the real cable is characterized by a structure of petals physically separated via steel wrapping, like for the ITER CS and TF conductors. Nevertheless, this is a fundamental addition to the capacity of the code since it might be used in the future to fine-tune the shaping process of any multistage cable. This model feature permitted describing twisted single-petal models with limited size and computation time, but also opened the way for full cable models. New objects, corresponding to the petals, were defined and implemented in the core of the code, so that the full cable model needs to specify the number of these components, their twist pitch and their helix radius. At the same time, helical surfaces have to be defined as for the single petal model. Fig. 1b) reports an example of the full cable model with sub-cables/petals separated by a wrapping. This final scale-up of the code permitted a completely new simulation approach, giving access to relevant information about the macroscopic mechanical phenomena occurring at the cable scale, as the ones presented in section III, which could not be described by the single petal/sub-cable model.

B. *Numerical protocol*

The upgrades and improvements of the model allowed the definition of a specific numerical protocol to simulate the main

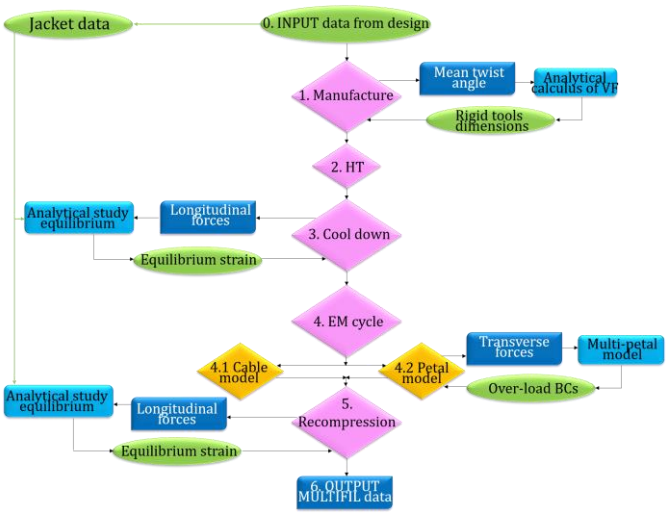

Fig. 2. Schematic drawing of the numerical protocol of the fusion cables simulations with MULTIFIL code.

phases of a fusion Nb_3Sn cable life by using MULTIFIL. This protocol identifies several numerical steps, alternated with analytical studies, to support and provide parameters necessary to the numerical simulations. A schematic of this procedure is reported in Fig. 2. The central pink rhombi represent the main steps of the cable life simulated by MULTIFIL; the details of each simulating step are given in [6]-[7]. The green ovals are the input data for the simulation provided by the design or the analytical routines (light blue rectangles) that post-process the data from the simulation (dark blue rectangles). For example, the final dimensions of the simulated cable/sub-cable are those producing the design Void Fraction (VF); to calculate it, the knowledge of the mean twist angle from the simulation is required, as explained in [10]. Also for the Cool-Down (CD) and EM cycle simulations it is necessary to find the mechanical equilibrium between the simulated cable and a virtual stainless steel jacket, as explained in [7] and [10], to account for the presence of the jacket. Moreover, the EM simulation is different if considering the single petal or the full cable model. In the first case, specific analytical formulae were developed for considering the presence of the other petals in the EM simulation [7].

III. ITER TF CICC FULL CABLE MODEL

A. *The test case*

The ITER TF CICC has been the reference test case for all the previous works [6], [7], [10] and so it was important to perform a deep mechanical analysis of this design by means of the full cable model. Indeed, this is the first time that it is possible to perform a simulation of the full geometry of a fusion conductor with MULTIFIL. The model is 150 mm long and refers to the data in Table I. Differently from the single petal model [10], the modelled mean twist angle corresponds now to the 0.97 value, as foreseen by the design, thanks to the presence of the last cabling stage. Even though the final VF is 29.7 % for both models, a different mean twist angle corresponds to a different mechanical behavior. In particular, in the longitudinal direction,

TABLE II
STRAIN BEHAVIOR OF ITER TF FULL CABLE MODEL FOR DIFFERENT LOADS

Loadings	ε_{ap} [%]	ε_{ax} [%]	γ^b [-]	ε_{pl} [%]	η^{pl} [-]
Cool Down	–0.672	–0.262	1.23	–0.177	2.09
1st EM cycle	–0.0676	–0.274	1.45	–0.282	37.10
4th EM cycle	–0.0169	–0.276	1.59	–0.288	24.41
5th EM cycle	–0.0169	–0.278	1.60	–0.290	24.79

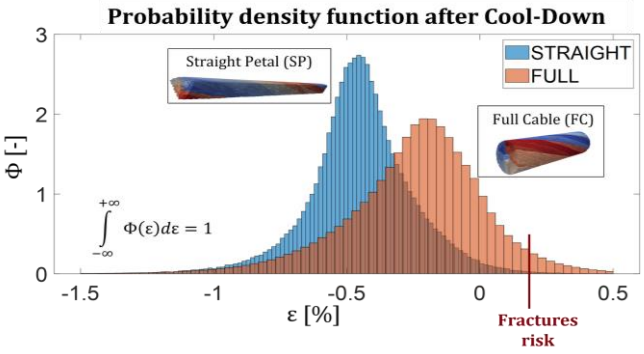

Fig. 3. Comparison of the probability density function distribution of strain after cool-down for the single straight petal model and the full cable model.

the full cable is softer than its single straight petal counterpart. In fact, the strain distribution after CD reported in Fig. 3 shows the ITER TF CICC for the single petal and full cable models. The only difference between the two models is the presence of the last cabling stage, but the distribution is more peaked and narrow for the single straight petal (STRAIGHT), with the mean value displaced towards the compressive strains comparable to the ITER Short Twist Pitch CS CICC behavior (see Fig. 6 of [11]). The distribution obtained with the full cable model (FULL) is broader and more exposed to bending, tensile strains and therefore to the risk of fracture as expected by this kind of cables (see Fig. 2 of [11]). The thermal strain applied to the cable (ε_{CD}) given by the jacket-cable equilibrium due to the CD is less compressive for the full cable model, which behaves as a "softer" cable.

B. *The main simulations and results*

By adopting the numerical protocol presented in Fig. 2, a first CD, followed by 5 EM cycles are performed.

In this paper, cumulative polar maps, which are the average of a given parameter for all the transverse cross-sections over the length of the cable, are reported to assess the evolution with loadings of some design parameters, such as the local twist angle and the local VF (Fig. 5) or physical values, like axial strain or contact forces (Fig. 6-7). Also the qualitative positioning of wires with cycles (Fig. 4) can be studied at a generic transverse cross-section of the cable length, for example at z = 75 mm.

Table II reports the evolution of some mechanical indicators defined in [10]. The first column represents the strain that the simulated cable undergoes due to the presence of the jacket, hence each loading adds a further strain whose contribution decreases with the loadings. The second parameter is the average axial strain (on the axis of the wires), that tends to become more compressive. The fourth column illustrates the evolution of the plastic contribution to the axial strain, which strongly increases

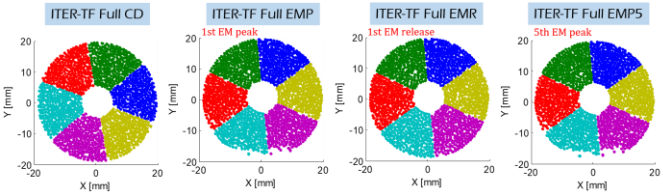

Fig. 4. For each loading, position of the wires over a generic cross-section at 75 mm of simulated cable length.

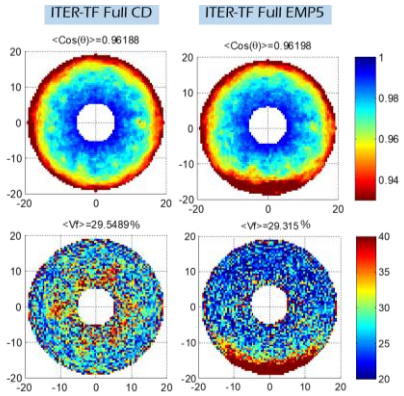

Fig. 5. First line: cumulative polar map of the mean twist angle for different loadings; second line: cumulative polar map of the local void fraction for different loadings.

with the application of the EM cycles. The bending and plastic ratios, third and fifth columns respectively, illustrate the repartition between the average bending and axial strains and the average plastic and elastic strains. This result highlights the plasticization due to the EM cycles and a global increase of the bending contribution.

C. *Discussion of the results*

The global behavior reported in Table II confirms the tendency observed for the single petal model in [10]. However, a major difference is related to the stiffer behavior of the single petal model, shown in Fig. 3, and to the bending ratios found in the two models. This ratio is below 1 for the petal model, which indicates a smaller contribution of the bending to the global strain with respect to the full cable model with values over 1.

For an EM force applied in the positive y-axis direction (vertical direction), the full cable model reveals the effect of the EM cycles on the wire displacement on the low EM pressure side, which was not detected by the petal model. At full EM load, the wires displacement is significant (few diameters), and a gap opens on the low-pressure side of the cable. Although the release of the EM load decreases this effect, some strands are plastically deformed and do not recover their initial position. A similar behavior was observed during destructive examination of the ITER CS CICCs tested sample JACS01 R [12]. Further experimental evidences on the VF behavior are presented in [13] and [14]. This phenomenon is also expressed by the local void fraction evolution illustrated in Fig. 5: the low EM pressure zone is characterized by a drastic increase of the local VF in the low EM pressure side, and by a subsequent reduction, more gradual, of the VF in the high pressure side, although the average values only marginally changes. Fig. 5 also shows the

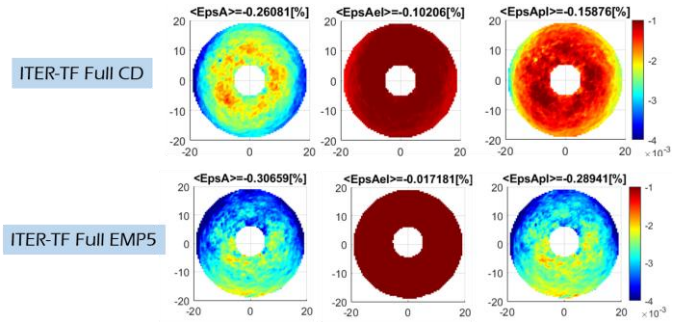

Fig. 6. First line: cumulative polar map of axial, elastic and plastic strains after CD; second line: cumulative polar map of axial, elastic and plastic strains at the 5th EM cycle peak.

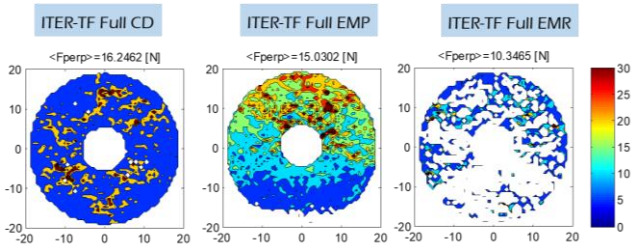

Fig. 7. Cumulative polar map of the perpendicular contact forces.

cross-sectional distribution of the local twist angle and highlights a localized increase of the buckling in the low EM pressure zone, corresponding to large displacements in this zone. This buckling was also observed experimentally on the low-pressure side of conductors opened after testing [12].

Fig. 6 reports the cumulative polar maps of axial, elastic and plastic strains. After CD, all strains are relatively axisymmetric on the cross-section. The effect of the EM cycles is a progressive increase of compressive plastic strains in the high EM pressure side, breaching the initial symmetry, while the elastic strain is marginal in the total axial strain. This global softening of the cable by plasticization relates with experimental measurements of null residual stress in the jacket in the high field zone of SULTAN sample [12].

Fig. 7 shows that the contact forces between strands tend to decrease or even disappear in the low EM pressure side of the cable. This drastic drop in contact force amplitude and contact number is another phenomenon revealed by this study. It demonstrates that this cable design (ITER-TF) is not able to maintain good contacts between strands during its operation, thus, probably, lessening its current redistribution capacity. This is in accordance to the drastic decrease of AC losses in ITER TF cables after cyclic loading (factor ~5-10 from [15]), and shows a phenomenon consistent with the direct measurements of inter-strand contact resistances performed by Twente [16].

IV. Other Conductor Designs

The main purpose of this section is to illustrate the versatility of the numerical protocol and MULTFIL model to simulate different Nb_3Sn CICCs: ITER CS CICC [15], JT60-SA CS CICC [17] and DTT TF CICC [18].

The Cu wires position (see the first line in Fig. 8) shows well the absence of Cu cores in the petals of JT-60SA CS and ITER

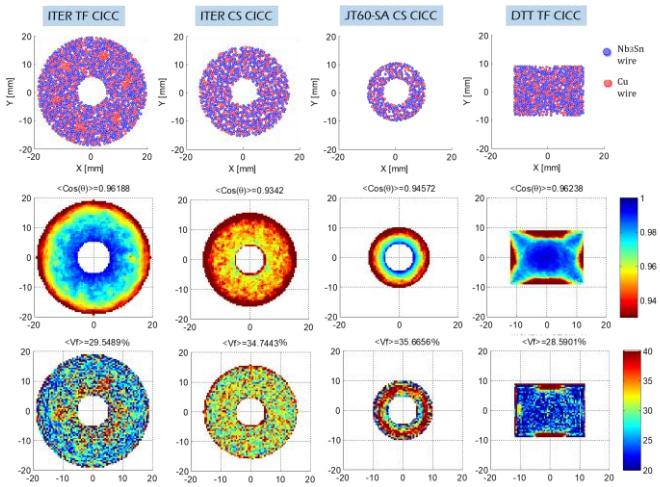

Fig. 8. First line: for each design, position of the Cu and Nb_3Sn wires over the cross-section at 75 mm; second line: cumulative polar map of local twist angle for different designs; third line: cumulative polar map of local void fraction for different designs.

CS CICCs with respect to the ITER TF CICC. The Cu cores are not visible for the DTT TF conductor: due to the high compaction of the DTT TF cable, the petals wires tend to mix with each other. The validity of this prediction should be verified by a direct examination of real DTT TF conductors. The different VF of the cables is visible as well (see the third line in Fig. 8). All the circular cables show, as expected from the cabling helices, a radial gradient presenting straighter wires towards the center of the cable (see Fig. 8, line 2). Clearly the ITER CS cable is characterized by a higher angle inclination with respect to the cable axis, due to its Short Twist Pitch (STP) design. An interesting distribution is shown by the rectangular geometry with straighter wires up to the cables corners. The three circular cables show a constant VF as a function of the angular coordinate. However, the maps present a completely different radial distribution depending on the test case, which indicates that the local VF distribution is also a function of the dimensions, as well as the average VF itself. Moreover, the local VF for the rectangular shows a particular distribution with minimum peaks corresponding to the angles.

V. Conclusion

The paper presents an important upgrade of the MUTLFIL code for the full geometry simulation of the ITER TF CICC in operation and a formalized protocol for the CICC simulations. The protocol was successfully adopted for the simulation of the geometry of different Nb_3Sn CICC designs. Future works will be focused on a comparative analysis of the mechanical behavior of these designs under electromechanical loadings.

A deeper study of the ITER TF CICC full cable model provided results consistent with experimental evidences and not represented by the single petal model. Particular attention was paid to the effect of the EM forces on the wires contacts and positioning, and consequently on the electrical contacts and resistances. Future studies will assess the electrical properties of the simulated cable as a function of the mechanical strain map.

REFERENCES

[1] N. Mitchell, "The ITER magnet system", *IEEE Transactions on Applied Superconductivity*, vol. 18, n°2, 2008.

[2] Y. Ilyin *et al*, "Scaling law for the strain dependence of the critical current in an advanced ITER Nb_3Sn strand", *Superconductor science and technology*, vol. 20, n°3, pp. 187-191, 2007.

[3] D. Ciazynski, "Review of Nb_3Sn conductors for ITER", *Fusion Engineering and Design*, vol. 82, issues 5-14, pp. 488-497, October 2007.

[4] M. Breschi *et al.*, "Peformance analysis of the toroidal field ITER production conductors", *Superconductor Science and Technology*, vol. 30, n°5, April 2017.

[5] H. Bajas *et al.*, "Finite element modelling of cable-in-conduit conductors", *Superconductor Science and Technology*, vol. 25, n°5, April 2012.

[6] R. Riccioli *et al.*, "Mechanical modeling and first case study on ITER TF CICC loading cases with upgraded finite element code simulations", *IEEE Transaction on Applied Superconductivity*, vol. 29, n°5, pp. 1-5, August 2019.

[7] R. Riccioli *et al.*, "Advanced mechanical modeling of cyclically loaded cable-in-conduit conductors for fusion magnets", *IEEE Transaction on Applied Superconductivity*, vol. 30, n°4, pp. 1-5, June 2020.

[8] D. Durville, "Numerical simulation of entangled materials mechanical properties", *Journal of Materials Sciences*, vol. 40, n°122, pp. 5941-5948, 2005.

[9] H. Bajas, "Numerical simulation of the mechanical behavior of the ITER cable-in-conduit conductors", *PHD thesis Ecole Centrale de Paris*, 2011.

[10] R. Riccioli *et al.*, "Study of the ITER TF CICC mechanical behavior under Cool-down and repetitive EM loadings", *IEEE Transaction on Applied Superconductivity*, vol. 31, n°5, pp. 1-5, August 2021.

[11] C. Calzolaio and P. Bruzzone, "Analysis of the CICC performance through the measurement of the thermal strain distribution of the Nb_3Sn filaments in the cable cross section", *IEEE Transaction on Applied Superconductivity*, vol. 24, n°3, June 2014.

[12] T. Hemmi *et al.*, "Test results and investigation of Tcs degradation in Japanese ITER CS conductor samples", *IEEE Transaction on Applied Superconductivity*, vol. 22, n°3, 2012.

[13] C. Sanabria *et al.*, "Metallographic autopsies of full-scale ITER prototype cable-in-conduit conductors after full testing in SULTAN: 1. The mechanical role of copper strands in a CICC", *Superconductor Science and Technology*, vol. 28, June 2015.

[14] C. Sanabria *et al.*, "Metallographic autopsies of full-scale ITER prototype cable-in-conduit conductors after full testing in SULTAN: II. Significant reduction of strand movement and strand damage in short twist pitch CICCs", *Superconductor Science and Technology*, vol. 28, October 2015.

[15] D. Bessette, "Design of a Nb_3Sn Cable-In-Conduit-Conductor to withstand the 60 000 electromagnetic cycles of the ITER central solenoid", *IEEE Transaction on Applied Superconductivity*, vol. 24, n°3, June 2014.

[16] A. Nijhuis *et al.*, "Change of interstrand contact resistance and coupling loss in various prototype ITER NbTi conductors with transverse loading in the twente cryogenic cable press up to 40,000 cycles", *Cryogenics*, vol. 44, issue 5, pp. 319-339, May 2004.

[17] K. Yoshida *et al*, "Design and Construction of JT-60SA Superconducting Magnet System", *J. Plasma Fusion Research*, 2010.

[18] L. Giannini *et al*, "Design Studies, Magnetic Calculations and Structural Assessment For the DTT Central Solenoid", *IEEE Transactions on Applied Superconductivity*, vol. 31, n°5, 2021.